ACS OMEGA

http://pubs.acs.org/journal/acsodf

Article

Coconut-Water-Mediated Carbonaceous Electrode: A Promising Eco-Friendly Material for Bifunctional Water Splitting Application

Siddheshwar D. Raut, Nanasaheb M. Shinde, Yogesh T. Nakate, Balaji G. Ghule, Shyam K. Gore, Shoyebmohamad F. Shaikh, James J. Pak,* Abdullah M. Al-Enizi,* and Rajaram S. Mane*

Cite This: *ACS Omega* 2021, 6, 12623−12630

Read Online

ACCESS | Metrics & More | Article Recommendations | Supporting Information

ABSTRACT: The organic and eco-friendly materials are extended to prevail over the worldwide energy crisis where bio-inspired carbonaceous electrode materials are being prepared from biogenic items and wastes. Here, coconut water is sprayed over three-dimensional (3D) nickel foam for obtaining a carbonaceous electrode material, i.e., C@Ni-F. The as-prepared C@Ni-F electrode has been used for structural elucidation and morphology evolution studies. Field emission scanning electron microscopy analysis confirms the vertically grown nanosheets of the C@Ni-F electrode, which is further employed in the oxygen evolution reaction (OER) and hydrogen evolution reaction (HER), where excellent OER and HER performances with small overpotentials of 219 and 122 mV and with stumpy Tafel slopes, i.e., 27 and 53 mV dec^{-1}, are respectively obtained, suggesting a bifunctional potential of the sprayed electrode material. Moreover, sustainable bifunctional performance of C@Ni-F proves considerable chemical stability and moderate mechanical robustness against long-term operation, suggesting that, in addition to being a healthy drink to mankind, coconut water can also be used for water splitting applications.

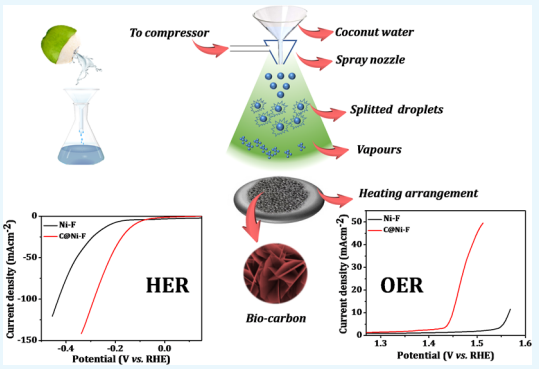

INTRODUCTION

Due to escalating demand of the clean and renewable energy caused by backdrop calamity and environmental pollution, the development of promising energy storage and conversion devices, i.e., catalysts, became obligatory.[1−3] Hydrogen is a promising option for clean energy, which can be produced by splitting water either in an electrocatalyzer or by photocatalysis. Electrochemical water splitting involves the hydrogen evolution reaction (HER) and oxygen evolution reaction (OER). Both reactions require a proper catalyst to boost the reaction kinetics.[4−6] So far, precious metals (Pt, Ru, and Pd) and noble metal oxides (IrO_2) showed the best performance toward both OER and HER. However, owing to the high cost and scarcity, they are obstructed.[7] Researchers have made several efforts to develop nonprecious metal-based catalysts for water splitting such as from sulfides,[8] selenides,[9] oxides,[10] etc. Among the known catalysts, carbon/carbonaceous electrode materials have demonstrated an excellent chemical and mechanical stability and porosity, high surface area, fine-controlled pore coordination, i.e., pore-size distribution and connectivity, good conductivity, low cost, and stability.[11] A variety of carbon materials with diverse morphologies and functionalities such as carbon nanotubes (CNTs),[12] fullerenes,[13] and graphene[14] were prepared by several physical and chemical methods. Most of the carbon/carbonaceous nanomaterials are reliant on fossil-based precursors, viz., pitch, coal, phenol, etc., which are expensive and detrimental to environmental health. Biomass, a rich, environmentally friendly, low-cost, renewable, novel, and abundant resource in nature, is an excellent source to prepare carbonaceous materials for scientific and practical benefits, reducing the environmental pollution greatly.[15] The animal- and plant-based materials are usually considered as biomass, which can be derived from nature.[16] Coconut is a preeminent biomass resource to prepare biocarbon as every part of coconut can be used to prepare biocarbon. Many researchers have prepared biocarbon from various parts of coconut, viz., shell,[17−19] leaves,[20] husk waste,[21] kernel,[22] etc. The biocarbon prepared using such biomass resources offers (i) relatively low internal resistance, (ii) superior electrical conductivity, (iii) outstanding cyclic stability, (iv) admirable chemical stability, and (v) excellent reaction kinetics.[17−22] Numerous synthesis techniques, i.e., hydrothermal technique, chemical bath deposition (CBD), electrodeposition, successive ionic layer adsorption and reaction (SILAR), and spray pyrolysis, were reported to prepare various biocarbon nanostructures in the form of a film/powder. Among them, spraying a direct solution over a

Received: February 4, 2021
Accepted: April 7, 2021
Published: May 10, 2021

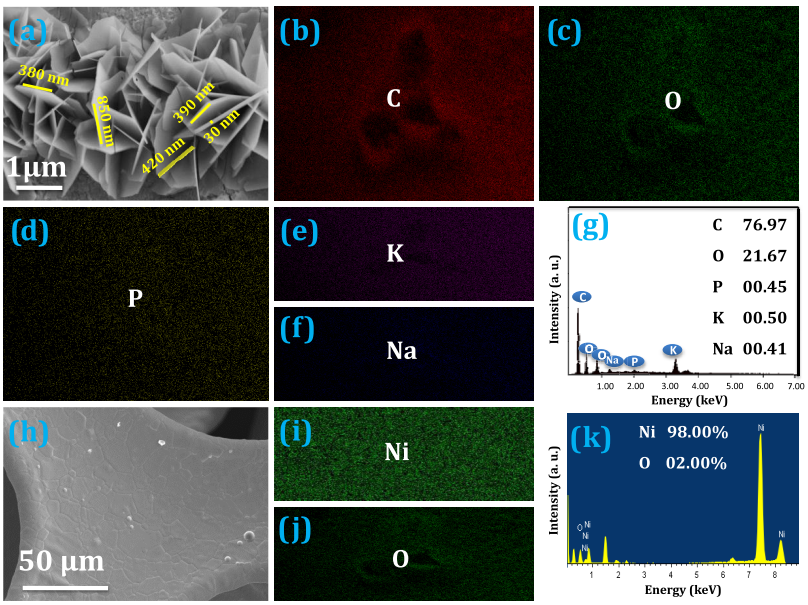

Figure 1. (a) FE-SEM image and (b–f) mapping images for C, O, P, K, and Na elements; (g) elements and their proportions obtained from the EDS spectrum of C@Ni-F; (h) FE-SEM image and (i, j) elemental mapping images of Ni and O; and (k) elemental composition of pristine Ni-F for knowing substrate specifications.

hot substrate for obtaining a film-type electrode is a cost-effective, safe, and uncomplicated synthesis technique to operate, by which the structure, phase, and morphology can be easily controlled by regulating various parameters such as, spray rate, operating temperature, flow rate, deposition time, etc.[23,24]

Prabu et al. reported the catalytic activity of activated carbon sheets prepared from bakery food waste toward OER and HER. The activated carbon-sheet electrode demonstrated both OER and HER activities with low overpotentials of 340 mV (at 10 mA cm^{-2}) and 380 mV (at −10 mA cm^{-2}), with corresponding Tafel slopes of 43 and 85 mV dec^{-1}.[25] Sathiskumar et al. prepared nitrogen-doped porous carbon (N-PC) from biomass, i.e., golden shower pod biomass (GSB), via a solvent-free strategy, which was further tested for electrolysis applications. The as-prepared N-PC electrode revealed admirable performance toward OER and HER with small overpotentials of 314 and 179 mV @ 10 mA cm^{-2} and low Tafel slopes of 132 and 98 mV dec^{-1}, respectively, in KOH electrolyte solution.[26] The catalytic performance of the bio-based carbon electrode can be determined through a three-dimensional porous structure, oxygen vacancies, and carbon defects. However, with such promising performances, still there is a lot of scope for the pioneering biogenic electrode materials with enhanced catalytic activities.

Herein, in continuation of our work[27] reporting a cost-effective, earth-abundant, and bio-inspired carbonaceous noble-metal-free electrode for clean and renewable energy, we have reported the use of sprayed coconut water over three-dimensional (3D) nickel foam, i.e., C@Ni-F, toward both OER and HER. The results obtained in this study were compared with those reported for the carbonaceous electrode derived from various biomasses for better understanding. Instead of other coconut parts, here, we have used sprayed coconut water for the first time for performing OER and HER.

MATERIAL CHARACTERIZATIONS

The structural elucidation and morphological evolution studies of the C@Ni-F electrode were attempted using X-ray diffraction (XRD, D8-Discovery Bruker, 40 kV, 40 mA, Cu Kα, λ = 1.5406 Å) and field emission scanning electron microscopy (FE-SEM, Hitachi, S-4800, 15 kV) with energy-dispersive X-ray spectroscopy (EDS) images, respectively. The surface chemical composition and the oxidation conditions were confirmed from X-ray photoelectron spectroscopy (XPS, VG Scientifics ESCALAB250) spectra. The functional groups present over the electrode surface were identified using a Fourier transform infrared spectroscopy (FTIR) plot. The Raman spectrophotometry (Xper Ram 200, Nano Base, South Korea) measurement was carried out to confirm the presence of the vibrational modes.

RESULTS AND DISCUSSION

Surface Appearance, Chemical Configuration Analysis, and Structural Elucidation. The FE-SEM image with EDS surface elemental composition is shown in Figure 1. The upright standing interconnected nanosheets were observed over plane Ni-F (discussed later) (Figure 1a). These interwoven-type nanosheets were 300–900 nm in length and 20–30 nm in thickness. There were several crevices between these nanosheets. The two side surfaces of these nanosheets were open, which would help to improve the reaction active area during the interaction with the electrolyte followed by proficient charge transportation for better performance. Moreover, as evidenced, bulky voids would defend the volume change, if any, while cycling.[29,30] The FE-SEM images of C@Ni-F and pristine Ni-F with different magnifications are shown in Figure S1. The elemental mapping images of as-prepared C@Ni-F are given in Figure 1b–f. The surface elemental composition of the C@Ni-F electrode as shown in Figure 1g showed carbon (C) and oxygen (O) as the major elements and phosphorous (P), potassium (K), and sodium (Na) in insignificant quantity due to which these elements were not

https://doi.org/10.1021/acsomega.1c00641
ACS Omega 2021, 6, 12623−12630

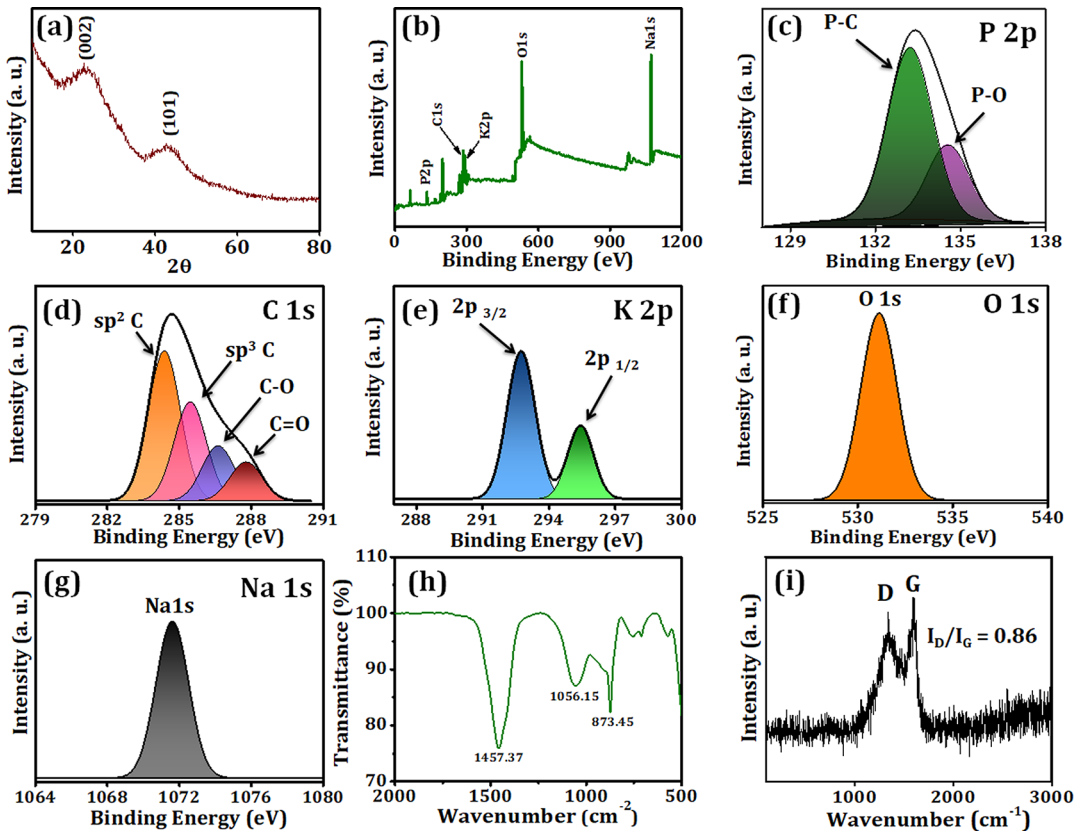

Figure 2. (a) XRD pattern; (b) survey and enlarged spectra for (c) P 2p, (d) C 1s, (e) K 2p, (f) O 1s, and (g) Na 1s; and (h) FTIR and (i) Raman spectra of C@Ni-F.

detected during structural analysis. The FE-SEM image of the bare Ni-F as shown in Figure 1h revealed the presence of only Ni and O elements (Figure 1i,j). The presence of oxygen could be due to a trace amount of environmental oxygen adsorbed over Ni-F.

The XRD pattern of the as-prepared C@Ni-F electrode is shown in Figure 2a, where two major peaks at 24.15 and 43.16° corresponding to the (002) and (101) reflection planes (JCPDS 41-1487) with interplanar spacings of 0.38 and 0.28 Å were, respectively, obtained, confirming the presence of carbon as the majority entity in the electrode material. The absence of peaks of other elements was due to their trace amount and low atomic numbers, which was also observed in XPS and EDAX analyses. The chemical structure and the oxidation conditions were obtained from the XPS spectra recorded for P, C, K, O, and Na elements (Figure 2b–g). Figure 2c presents deconvoluted P 2p peaks of P–C and P–O bonds at, respectively, 133.3 and 134.4 eV binding energies.[31−33] The deconvoluted C 1s spectrum with four Gaussian curves as shown in Figure 2d revealed the sp^2 carbon, sp^3 carbon, C–O, and C═O bondings at 284.55, 285.51, 286.6, and 287.77 eV, respectively.[34−36] The as-observed peaks were of hydroxyl (C═C/C–C) and epoxy groups (C–O), suggesting the presence of oxygen-containing groups in the form of epoxy and hydroxyl groups, which is in good agreement with the Lerf–Klinowski model of carbonaceous electrodes.[37,38] Figure 2e shows the K 2p spectrum with spin energy partition of 2.8 eV, where two major peaks are evidenced at 292.7 and 295.5 eV for the K $2p_{3/2}$ and K $2p_{1/2}$ levels, respectively.[39] The peak observed at 531.01 eV in O 1s spectra was for C–O–C[40] (Figure 2f). A single broad deconvoluted peak of Na 1s is also observed in Figure 2g at 271.5 eV, suggesting the presence of Na^+.[41]

The existence of the functional groups on the electrode surface was confirmed using the FTIR spectrum (Figure 2h). The band observed at 1457.37 cm^{-2} was attributed to the plane deformation vibrations of the C–H moiety in $-CH_3$, $-CH_2-$, and $-O-CH_3$.[42] The peak at 1056.15 cm^{-2} was due to the saccharide structure of cellulose and hemicelluloses, and the peak at 873.45 cm^{-2} was assigned to the bending vibrations of the aromatic compounds.[43,44] The Raman spectrum as shown in Figure 2i confirmed two peaks at 1355.66 and 1582.85 cm^{-2} for D and G bands, respectively.[45] The observed D band indicated the disorder in the carbon structure with A_{1g} symmetry, while the G band showed the C═C stretching vibration with E_{2g} mode. The I_D/I_G ratio was found to be 0.86, providing information about the crystallite dimension, plane defects, edge defects, and the nature of disorder of the carbon derivative.[46] It is confirmed that the presence of K, P, and Na in C@Ni-F could be responsible for the enhancement in the formation of defects, which results in the increasing intensity of the G band following incorporation of –OH groups in the layered structures for better performance.[47,48]

Electrochemical Measurements. The electrochemical properties of the C@Ni-F electrode were studied using an IVIUM electrochemical workstation by employing a three-electrode system: platinum as a counter electrode, Ag/AgCl as a reference electrode, and deposited Ni-F as a working electrode. The OER polarization curves were obtained in a 1.0 M KOH electrolyte and compared with that of bare Ni-F for assessing the performance of the sprayed carbonaceous electrode material only.

https://doi.org/10.1021/acsomega.1c00641
ACS Omega 2021, 6, 12623−12630

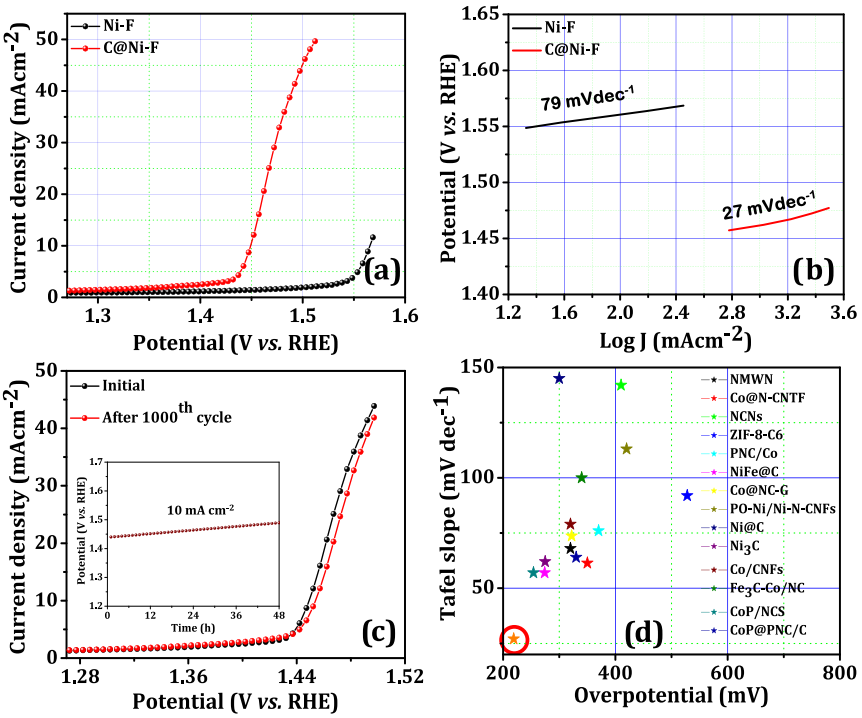

Figure 3. (a) OER polarization curves, (b) Tafel plots, (c) cyclic stability (inset shows chemical stability), and (d) comparison graph of OER activity of C@Ni-F with former data (the red circle indicates the overpotential and Tafel slope of the current work).

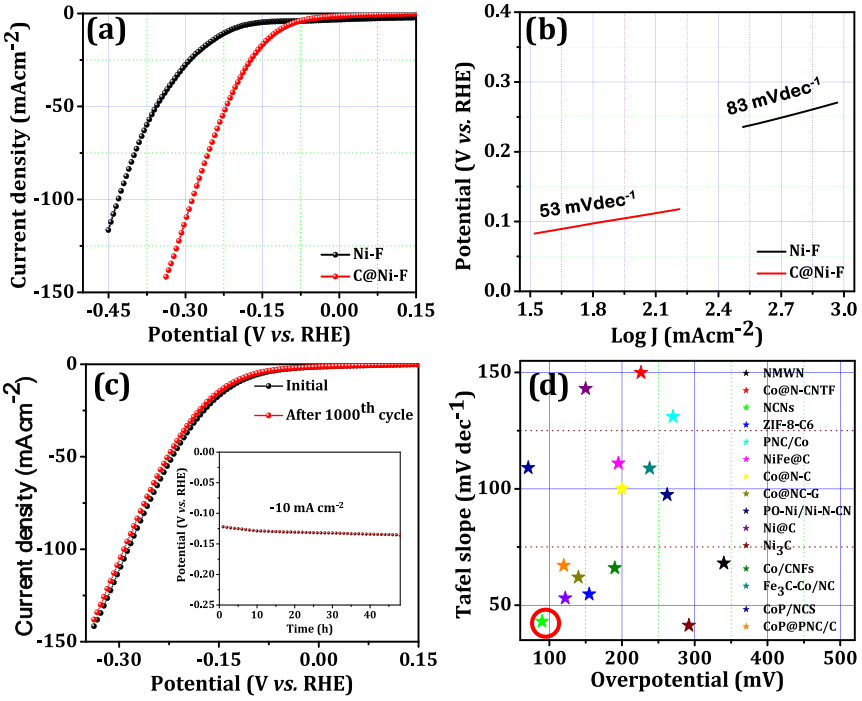

Figure 4. (a) HER polarization curves, (b) Tafel plots, (c) cyclic stability (inset shows chemical stability), and (d) performance comparison of the HER activity of C@Ni-F with survey data (the red circle indicates the overpotential and Tafel slope of the current work).

Oxygen and Hydrogen Evolution Study. The polarization curves of C@Ni-F showed a promising OER activity with a small overpotential (η) of 219 mV, calculated by eq 2 in the Supporting Information, which is much inferior to the overpotential of Ni-F, i.e., 330 mV (Figure 3a) at a current density of 10 mA cm^{-2}. The Tafel slopes (determined using eq 3 in the Supporting Information) of C@Ni-F and Ni-F electrodes, extracted from the polarization curves, are shown in Figure 3b. The OER kinetics of the C@Ni-F electrode can be understood using Tafel plots. The lower Tafel slope specifies the good reaction kinetics. Herein, the C@Ni-F electrode presented the smallest Tafel slope of 27 mV dec^{-1}, while Ni-F revealed 79 mV dec^{-1}, which indicates the superior reaction kinetics of the previous electrode toward OER over the latter one.[49] The cyclic and chemical stability of C@Ni-F was verified with continuous OER at a fixed potential and is shown

https://doi.org/10.1021/acsomega.1c00641
ACS Omega 2021, 6, 12623−12630

Table 1. Comparison of Electrochemical Properties of C@Ni-F with Carbonaceous Electrodes

		η (mV)/Tafel slope (mV dec^{-1})			
catalyst	electrolyte	OER	HER	J (mA cm^{-2})	ref
NMWN	1.0 M NaOH	320/68	340/68	10	51
Co@N-CNTF	1.0 M KOH	350/61.4	226/149.9	10	52
NCNs	1.0 M KOH/0.5 M H_2SO_4	410/142	90/43	10	53
ZIF-8-C6	0.1 M KOH/0.5 M H_2SO_4	528/91.9	155/54.7	10	54
PNC/Co	1.0 M KOH	370/76	270/131	10	55
NiFe@C	1.0 M KOH	274/57	195/111	10	56
Co@N-C	1.0 M KOH	400/−	200/100	10	57
Co@NC-G	1.0 M KOH	322/73.7	140/62	10	58
PO-Ni/Ni-N-CNFs	1.0 M KOH	420/113.10	262/97.42	10	59
Ni@C	1.0 M KOH	300/145	150/143	10	60
Ni_3C	1.0 M KOH	275/62	292/41.3	10	61
Co/CNFs	1.0 M KOH	320/79	190/66	10	62
Fe_3C-Co/NC	1.0 M KOH/0.5 M H_2SO_4	340/100	238/108.8	10	63
CoP/NCS	1.0 M KOH	254/57	71/109	10	64
CoP@PNC/C	1.0 M KOH	330/64	120/67	10	65
C@Ni-F	1.0 M KOH	219/27	122/53	10	present work

in Figure 3c. The as-prepared C@Ni-F electrode demonstrated excellent cyclic and chemical stability. The C@Ni-F electrode revealed mostly stable current density after 1000 cycles and 48 h for long-term cycling and chemical stability (inset of Figure 3c). After 1000 cycles, a minute change of just 4 mV, i.e., 98.20% retention, was observed in the overpotential of the C@Ni-F electrode. The OER activity of the as-obtained C@Ni-F electrode was comparable to the performance of previously reported carbonaceous electrode materials, which is graphically shown in Figure 3d.

The HER activity of the C@Ni-F electrode as shown in Figure 4 was carried out under analogous conditions to OER. The polarization curve of C@Ni-F showed admirable activity toward HER with petite overpotential of 122 mV, whereas Ni-F revealed an overpotential of 220 mV at a current density of −10 mA cm^{-2} (Figure 4a). The corresponding Tafel slopes, an intrinsic property of electrocatalysts, extracted from HER polarization curves of C@Ni-F and pristine Ni-F are shown in Figure 4b. A smaller Tafel slope indicates a higher HER rate, and a Tafel slope as small as 53 mV dec^{-1} signifies that the HER obeys the Volmer−Heyrovsky mechanism on the electrode surface.[50] The cyclic and chemical stability of the C@Ni-F electrode is shown in Figure 4c. After 1000 cycling operations, the C@Ni-F electrode showed an excellent stability (94.57% retention) with insignificant variation in overpotential, showing almost stable performance even after 48 h (inset of Figure 4c). The comparative performance of the C@Ni-F electrode toward HER has been graphically represented in Figure 4d and is given in Table 1.[51−65]

Conclusions and Perspectives. In this work, we successfully prepared vertically grown C@Ni-F nanosheet electrodes using the facile spray pyrolysis synthesis method over a Ni-F substrate. The XRD patterns confirmed the formation of the C@Ni-F electrode, while the elements present on the electrode surface were verified using XPS. The surface bands and functional groups were confirmed by Raman and FTIR spectroscopies, which confirmed the formation of C@Ni-F. The as-prepared C@Ni-F electrode on employing in electrochemical measurements for OER and HER water splitting applications showed lower overpotentials and smaller Tafel slopes. The OER overpotential of the C@Ni-F electrode was 219 mV, while for HER, it was 122 mV. The C@Ni-F electrode, with the small overpotential toward both OER (27 mV dec^{-1}) and HER (53 mV dec^{-1}), showed good reaction kinetics. This admirable performance of the C@Ni-F electrode is attributing to a high surface area, upright standing platelet surface morphology that facilitates east and easy charge transfer processing, and availability of bounteous active sites sowing to interconnected porous nanosheets network. A C@Ni-F electrode was obtained at one side of the substrate surface only, forming a bisprayed surface with metal oxides, polymers, and carbonaceous materials on the other side would open a new research avenue in energy storage and water splitting devices for manufacturing various technologies.

EXPERIMENTAL SECTION

Materials. Fresh young coconuts from Partur, Maharashtra, India, and deionized (DI) water and Ni-F-110 with 320 g m^{-2} mass density from Artenano Company Limited, Hong Kong, were purchased and used after cleaning.

Spraying of Coconut Water. The coconut-water-mediated carbonaceous electrode was prepared using the spray pyrolysis method with the protocol reported earlier.[28] Coconut water was collected from fresh kernel-free green coconut, which was further filtered using Whatman filter paper to avoid any solid impurity. Ni-F (1 cm × 4 cm × 0.1 mm) was used as a substrate, which was cleaned by 1.0 M HCL solution, DI water, and ethanol for 15 min each with ultrasonication to avoid impurity additives. Afterward, the filtered coconut water was poured into the solution dispenser of the spray pyrolysis instrument (HOLMARC HO-TH-04, India), which was connected to and operated by a personal computer. A cleaned 3D Ni-F substrate was kept on a hot plate by adjusting the X−Y coordinates appropriately. The temperature of the hot plate was optimized to 150 °C using a controller.

Furthermore, spraying was conducted with a flow rate of 2 mL min^{-1} and air-flow rate of 15 L min^{-1} in a closed chamber for 14 min. After deposition, the substrate temperature was allowed to return to room temperature naturally to avoid the quenching effect. Finally, the prepared deposited electrode Ni-F was annealed at 400 °C before applying for further electrochemical measurements. The schematic of the experimental setup used to synthesize C@Ni-F is shown in Scheme 1.

https://doi.org/10.1021/acsomega.1c00641
ACS Omega 2021, 6, 12623−12630

Scheme 1. Schematic of Obtaining a Carbon Film with a Platelet Architecture on Spraying Coconut Water on Ni-F

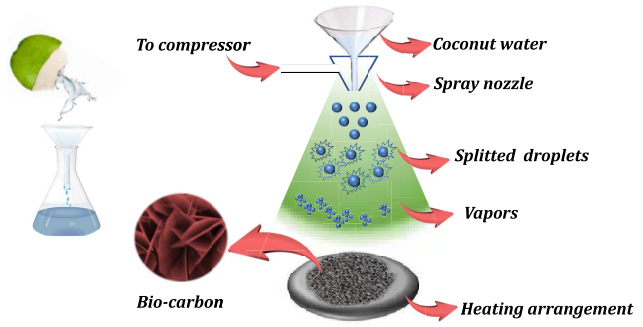

■ ASSOCIATED CONTENT

Supporting Information

The Supporting Information is available free of charge at https://pubs.acs.org/doi/10.1021/acsomega.1c00641.

Equations and FE-SEM images of bare Ni-foam and C@Ni-F at different magnifications (PDF)

■ AUTHOR INFORMATION

Corresponding Authors

James J. Pak − *School of Electrical Engineering, Korea University, Seoul 02841, Republic of Korea;* orcid.org/0000-0003-2141-9452; Email: pak@korea.ac.kr

Abdullah M. Al-Enizi − *Department of Chemistry, College of Science, King Saud University, Riyadh 11451, Saudi Arabia;* orcid.org/0000-0002-3967-5553; Email: amenizi@ksu.edu.sa

Rajaram S. Mane − *School of Physical Sciences, Swami Ramanand Teerth Marathwada University, Nanded 431501, Maharashtra, India;* orcid.org/0000-0002-9624-7985; Email: rajarammane70@srtmun.ac.in

Authors

Siddheshwar D. Raut − *School of Physical Sciences, Swami Ramanand Teerth Marathwada University, Nanded 431501, Maharashtra, India*

Nanasaheb M. Shinde − *School of Electrical Engineering, Korea University, Seoul 02841, Republic of Korea*

Yogesh T. Nakate − *Department of Electronics, Kavayitri Bahinabai Chaudhari North Maharashtra University, Jalgaon 425001, Maharashtra, India*

Balaji G. Ghule − *School of Physical Sciences, Swami Ramanand Teerth Marathwada University, Nanded 431501, Maharashtra, India;* orcid.org/0000-0002-4746-0296

Shyam K. Gore − *Dnyanopasak Shikshan Mandal's Arts, Commerce and Science College, Jintur 431509, India*

Shoyebmohamad F. Shaikh − *Department of Chemistry, College of Science, King Saud University, Riyadh 11451, Saudi Arabia;* orcid.org/0000-0002-2137-324X

Complete contact information is available at: https://pubs.acs.org/10.1021/acsomega.1c00641

Notes

The authors declare no competing financial interest.

■ ACKNOWLEDGMENTS

The authors would like to extend their sincere appreciation to the Researchers supporting project number (RSP-2021/55), King Saud University, Riyadh, Saudi Arabia for financial support.

■ ABBREVIATIONS

NMWN, nitrogen-doped multi-walled carbon nanotube; **Co@N-CNTF**, cobalt nanoparticle-embedded nitrogen-doped carbon/carbon nanotube framework; **NCNs**, nitrogen-doped ultrathin carbon nanosheets; **ZIF-8-C6**, zeolitic imidazolate framework-8-derived carbon material; **PNC/Co**, porous N-rich carbon derived from a cobalt-containing metal-organic framework; **NiFe@C**, carbon-layer-encapsulated NiFe nanoparticles; **Co@N-C**, cobalt nanoparticles encapsulated in nitrogen-doped carbon; **Co@NC-G-Co/CoO$_x$**, nanoparticles embedded into nitrogen-doped carbon-graphene; **PO-Ni/Ni-N-CNFs**, partially oxidized Ni nanoparticles supported on Ni-N codoped carbon nanofibers; **Ni@C**, carbon-coated nickel; **Co/CNFs**, cobalt nanoparticle-encapsulated 3D conductive films; **Fe$_3$C-Co/NC**, Fe$_3$C and Co nanoparticles encapsulated in a nanoporous hierarchical structure of N-doped carbon; **CoP/NCS**, CoP particles embedded in N-doped carbon sheets; **CoP@PNC/C**, cobalt phosphide nanoparticles embedded in P and N codoped carbon (PNC) matrix with carbon black

■ REFERENCES

(1) Dai, M.; Zhao, D.; Liu, H.; Tong, Y.; Hu, P.; Wu, X. Nanostructure and doping engineering of ZnCoP for high performance electrolysis of water. *Mater. Today Eng.* **2020**, *16*, No. 100412.

(2) Sun, H.; Yan, Z.; Liu, F.; Xu, W.; Cheng, F.; Chen, J. Self-supported transition-metal-based electrocatalysts for hydrogen and oxygen evolution. *Adv. Mater.* **2020**, *32*, No. 1806326.

(3) Asset, T.; Job, N.; Busby, Y.; Crisci, A.; Martin, V.; Stergiopoulos, V.; Bonnaud, C.; Serov, A.; Atanassov, P.; Chattot, R.; Dubau, L.; et al. Porous hollow PtNi/C electrocatalysts: carbon support considerations to meet performance and stability requirements. *ACS Catal.* **2018**, *8*, 893−903.

(4) Zhao, D.; Dai, M.; Zhao, Y.; Liu, H.; Liu, Y.; Wu, X. Improving electrocatalytic activities of $FeCo_2O_4$@$FeCo_2O_4$@PPy electrodes by surface/interface regulation. *Nano Energy* **2020**, *72*, No. 104715.

(5) Tao, L.; Wang, Y.; Zou, Y.; Zhang, N.; Zhang, Y.; Wu, Y.; Wang, Y.; Chen, R.; Wang, S. Charge Transfer Modulated Activity of Carbon-Based Electrocatalysts. *Adv. Energy Mater.* **2020**, *10*, No. 1901227.

(6) Zhao, Y.; Nakamura, R.; Kamiya, K.; Nakanishi, S.; Hashimoto, K. Nitrogen-doped carbon nanomaterials as non-metal electrocatalysts for water oxidation. *Nat. Commun.* **2013**, *4*, No. 2390.

(7) Zhao, D.; Dai, M.; Liu, H.; Chen, K.; Zhu, X.; Xue, D.; Wu, X.; Liu, J. Sulfur-Induced Interface Engineering of Hybrid $NiCo_2O_4$@$NiMo_2S_4$ Structure for Overall Water Splitting and Flexible Hybrid Energy Storage. *Adv. Mater. Interfaces* **2019**, *6*, No. 1901308.

(8) Shinde, N.; Shinde, P.; Xia, Q. X.; Yun, J. M.; Mane, R.; Kim, K. H. Electrocatalytic Water Splitting through the Ni_xS_y Self-Grown Superstructures Obtained via a Wet Chemical Sulfurization Process. *ACS Omega* **2019**, *4*, 6486−6491.

(9) Wu, H.; Lu, X.; Zheng, G.; Ho, G. W. Topotactic engineering of ultrathin 2D nonlayered nickel selenides for full water electrolysis. *Adv. Energy Mater.* **2018**, *8*, No. 1702704.

(10) Raut, S. D.; Mane, H. R.; Shinde, N. M.; Lee, D.; Shaikh, S. F.; Kim, K. H.; Kim, H. J.; Al-Enizi, A. M.; Mane, R. S. Electrochemically grown MnO_2 nanowires for supercapacitor and electrocatalysis applications. *New J. Chem.* **2020**, *44*, 17864−17870.

(11) Shen, K.; Chen, X.; Chen, J.; Li, Y. Development of MOF-derived carbon-based nanomaterials for efficient catalysis. *ACS Catal.* **2016**, *6*, 5887−5903.

(12) Peigney, A.; Laurent, C.; Flahaut, E.; Bacsa, R. R.; Rousset, A. Specific surface area of carbon nanotubes and bundles of carbon nanotubes. *Carbon* **2001**, *39*, 507−514.

(13) Dai, L.; Chang, D. W.; Baek, J. B.; Lu, W. Carbon nanomaterials for advanced energy conversion and storage. *Small* **2012**, *8*, 1130−1166.
(14) Novoselov, K. S.; Geim, A. K.; Morozov, S. V.; Jiang, D.; Zhang, Y.; Dubonos, S. V.; Grigorieva, I. V.; Firsov, A. A. Electric field effect in atomically thin carbon films. *Science* **2004**, *306*, 666−669.
(15) Bi, Z.; Kong, Q.; Cao, Y.; Sun, G.; Su, F.; Wei, X.; Li, X.; Ahmad, A.; Xie, L.; Chen, C. M. Biomass-derived porous carbon materials with different dimensions for supercapacitor electrodes: a review. *J. Mater. Chem. A* **2019**, *7*, 16028−16045.
(16) Lu, H.; Zhao, X. S. Biomass-derived carbon electrode materials for supercapacitors. *Sustainable Energy Fuels* **2017**, *1*, 1265−1281.
(17) Xia, J.; Zhang, N.; Chong, S.; Chen, Y.; Sun, C.; et al. Three-dimensional porous graphene-like sheets synthesized from biocarbon via low-temperature graphitization for a supercapacitor. *Green Chem.* **2018**, *20*, 694−700.
(18) Sun, L.; Tian, C.; Li, M.; Meng, X.; Wang, L.; Wang, R.; Yin, J.; Fu, H. From coconut shell to porous graphene-like nanosheets for high-power supercapacitors. *J. Mater. Chem. A* **2013**, *1*, 6462−6470.
(19) Jain, A.; Aravindan, V.; Jayaraman, S.; Kumar, P. S.; Balasubramanian, R.; Ramakrishna, S.; Madhavi, S.; Srinivasan, M. P. Activated carbons derived from coconut shells as high energy density cathode material for Li-ion capacitors. *Sci. Rep.* **2013**, *3*, No. 3002.
(20) Sulaiman, K. S.; Mat, A.; Arof, A. K. Activated carbon from coconut leaves for electrical double-layer capacitor. *Ionics* **2016**, *22*, 911−918.
(21) Taer, E.; Taslim, R.; Putri, A. W.; Apriwandi, A.; Agustino, A. Activated carbon electrode made from coconut husk waste for supercapacitor application. *Int. J. Electrochem. Sci.* **2018**, *13*, 12072−12084.
(22) Kishore, B.; Shanmughasundaram, D.; Penki, T. R.; Munichandraiah, N. Coconut kernel-derived activated carbon as electrode material for electrical double-layer capacitors. *J. Appl. Electrochem.* **2014**, *44*, 903−916.
(23) Perednis, D.; Gauckler, L. J. Thin film deposition using spray pyrolysis. *J. Electroceram.* **2005**, *14*, 103−111.
(24) Teli, A. M.; Bekanalkar, S. A.; Patil, D. S.; Pawar, S. A.; Dongale, T. D.; Shin, J. C.; Kim, H. J.; Patil, P. S. Effect of thermal annealing on physiochemical properties of spray-deposited β-MnO_2 thin films for electrochemical supercapacitor. *J. Electroanal. Chem.* **2020**, *856*, No. 113483.
(25) Prabu, N.; Kesavan, T.; Maduraiveeran, G.; Sasidharan, M. Bio-derived nanoporous activated carbon sheets as electrocatalyst for enhanced electrochemical water splitting. *Int. J. Hydrogen Energy* **2019**, *44*, 19995−20006.
(26) Sathiskumar, C.; Ramakrishnan, S.; Vinothkannan, M.; Karthikeyan, S.; Yoo, D. J.; et al. Nitrogen-doped porous carbon derived from biomass used as trifunctional electrocatalyst toward oxygen reduction, oxygen evolution and hydrogen evolution reactions. *Nanomaterials* **2020**, *10*, No. 76.
(27) Ghule, B. G.; Shinde, N. M.; Raut, S. D.; Shaikh, S. F.; Al-Enizi, A. M.; Kim, K. H.; Mane, R. S. Porous metal-graphene oxide nanocomposite sensors with high ammonia detectability. *J. Colloid Interface Sci.* **2021**, *589*, 401−410.
(28) Perednis, D.; Gauckler, L. J. Thin film deposition using spray pyrolysis. *J. Electroceram.* **2005**, *14*, 103−111.
(29) Xia, T.; Wang, Y.; Mai, C.; Pan, G.; Zhang, L.; Zhao, W.; Zhang, J. Facile in situ growth of ZnO nanosheets standing on Ni foam as binder-free anodes for lithium ion batteries. *RSC Adv.* **2019**, *9*, 19253−19260.
(30) Sun, H.; Luo, M.; Weng, W.; Cheng, K.; Du, P.; Shen, G.; Han, G. Room-temperature preparation of ZnO nanosheets grown on Si substrates by a seed-layer assisted solution route. *Nanotechnology* **2008**, *19*, No. 125603.
(31) Yuan, C. Z.; Jiang, Y. F.; Wang, Z.; Xie, X.; Yang, Z. K.; Yousaf, A. B.; Xu, A. W. Cobalt phosphate nanoparticles decorated with nitrogen-doped carbon layers as highly active and stable electro-catalysts for the oxygen evolution reaction. *J. Mater. Chem. A* **2016**, *4*, 8155−8160.
(32) Anwar, A.; Rehman, I. U.; Darr, J. A. Low-temperature synthesis and surface modification of high surface area calcium hydroxyapatite nanorods incorporating organofunctionalized surfaces. *J. Phys. Chem. C* **2016**, *120*, 29069−29076.
(33) Hu, X.; Li, R.; Zhao, S.; Xing, Y. Microwave-assisted preparation of flower-like cobalt phosphate and its application as a new heterogeneous Fenton−like catalyst. *Appl. Surf. Sci.* **2017**, *396*, 1393−1402.
(34) Dwivedi, N.; Yeo, R. J.; Satyanarayana, N.; Kundu, S.; Tripathy, S.; Bhatia, C. S. Understanding the role of nitrogen in plasma-assisted surface modification of magnetic recording media with and without ultrathin carbon overcoats. *Sci. Rep.* **2015**, *5*, No. 7772.
(35) Goohpattader, P. S.; Dwivedi, N.; Rismani-Yazdi, E.; Satyanarayana, N.; Yeo, R. J.; Kundu, S.; Bhatia, C. S. Probing the role of C+ ion energy, thickness and graded structure on the functional and microstructural characteristics of ultrathin carbon films (<2 nm). *Tribol. Int.* **2015**, *81*, 73−88.
(36) Yeo, R. J.; Rismani, E.; Dwivedi, N.; Blackwood, D. J.; Tan, H. R.; Zhang, Z.; Tripathy, S.; Bhatia, C. S. Bi-level surface modification of hard disk media by carbon using filtered cathodic vacuum arc: Reduced overcoat thickness without reduced corrosion performance. *Diamond Relat. Mater.* **2014**, *44*, 100−108.
(37) Dolgov, A.; Lopaev, D.; Lee, C. J.; Zoethout, E.; Medvedev, V.; Yakushev, O.; Bijkerk, F. Characterization of carbon contamination under ion and hot atom bombardment in a tin-plasma extreme ultraviolet light source. *Appl. Surf. Sci.* **2015**, *353*, 708−713.
(38) Lerf, A.; He, H.; Forster, M.; Klinowski, J. Structure of graphite oxide revisited. *J. Phys. Chem. B* **1998**, *102*, 4477−4482.
(39) Li, S.; Kang, E. T.; Neoh, K. G.; Ma, Z. H.; Tan, K. L.; Huang, W. In situ XPS studies of thermally deposited potassium on poly (p-phenylenevinylene) and its ring-substituted derivatives. *Appl. Surf. Sci.* **2001**, *181*, 201−210.
(40) Sivaranjini, B.; Mangaiyarkarasi, R.; Ganesh, V.; Umadevi, S. Vertical alignment of liquid crystals over a functionalized flexible substrate. *Sci. Rep.* **2018**, *8*, No. 8891.
(41) Geng, H. Z.; Kim, K. K.; So, K. P.; Lee, Y. S.; Chang, Y.; Lee, Y. H. Effect of acid treatment on carbon nanotube-based flexible transparent conducting films. *J. Am. Chem. Soc.* **2007**, *129*, 7758−7759.
(42) Huang, Y.; Ma, E.; Zhao, G. Thermal and structure analysis on reaction mechanisms during the preparation of activated carbon fibers by KOH activation from liquefied wood-based fibers. *Ind. Crops Prod.* **2015**, *69*, 447−455.
(43) Angin, D. Production and characterization of activated carbon from sour cherry stones by zinc chloride. *Fuel* **2014**, *115*, 804−811.
(44) Sharma, A.; Siddiqui, Z. M.; Dhar, S.; Mehta, P.; Pathania, D. Adsorptive removal of congo red dye (CR) from aqueous solution by Cornulacamonacantha stem and biomass-based activated carbon: isotherm, kinetics and thermodynamics. *Sep. Sci. Technol.* **2019**, *54*, 916−929.
(45) Li, Q. Q.; Zhang, X.; Han, W. P.; Lu, Y.; Shi, W.; Wu, J. B.; Tan, P. H. Raman spectroscopy at the edges of multilayer graphene. *Carbon* **2015**, *85*, 221−224.
(46) Kumar, M. P.; Kesavan, T.; Kalita, G.; Ragupathy, P.; Narayanan, T. N.; Pattanayak, D. K. On the large capacitance of nitrogen doped graphene derived by a facile route. *RSC Adv.* **2014**, *4*, 38689−38697.
(47) Cançado, L. G.; Jorio, A.; Ferreira, E. M.; Stavale, F.; Achete, C. A.; Capaz, R. B.; Moutinho, M. V. D. O.; Lombardo, A.; Kulmala, T. S.; Ferrari, A. C. Quantifying defects in graphene via Raman spectroscopy at different excitation energies. *Nano Lett.* **2011**, *11*, 3190−3196.
(48) Pimenta, M. A.; Dresselhaus, G.; Dresselhaus, M. S.; Cancado, L. G.; Jorio, A.; Saito, R. Studying disorder in graphite-based systems by Raman spectroscopy. *Phys. Chem. Chem. Phys.* **2007**, *9*, 1276−1290.

https://doi.org/10.1021/acsomega.1c00641
ACS Omega 2021, 6, 12623−12630

(49) Xia, B. Y.; Yan, Y.; Li, N.; Wu, H. B.; Lou, X. W. D.; Wang, X. A metal−organic framework-derived bifunctional oxygen electrocatalyst. *Nat. Energy* **2016**, *1*, No. 15006.
(50) Deng, J.; Ren, P.; Deng, D.; Yu, L.; Yang, F.; Bao, X. Highly active and durable non-precious-metal catalysts encapsulated in carbon nanotubes for hydrogen evolution reaction. *Energy Environ. Sci.* **2014**, *7*, 1919−1923.
(51) Davodi, F.; Tavakkoli, M.; Lahtinen, J.; Kallio, T. Straightforward synthesis of nitrogen-doped carbon nanotubes as highly active bifunctional electrocatalysts for full water splitting. *J. Catal.* **2017**, *353*, 19−27.
(52) Guo, H.; Feng, Q.; Zhu, J.; Xu, J.; Li, Q.; Liu, S.; Xu, K.; Zhang, C.; Liu, T. Cobalt nanoparticle-embedded nitrogen-doped carbon/carbon nanotube frameworks derived from a metal−organic framework for tri-functional ORR, OER and HER electrocatalysis. *J. Mater. Chem. A* **2019**, *7*, 3664−3672.
(53) Jiang, H.; Gu, J.; Zheng, X.; Liu, M.; Qiu, X.; Wang, L.; Li, W.; Chen, Z.; Ji, X.; Li, J. Defect-rich and ultrathin N doped carbon nanosheets as advanced trifunctional metal-free electrocatalysts for the ORR, OER and HER. *Energy Environ. Sci.* **2019**, *12*, 322−333.
(54) Lei, Y.; Wei, L.; Zhai, S.; Wang, Y.; Karahan, H. E.; Chen, X.; Zhou, Z.; Wang, C.; Sui, X.; Chen, Y. Metal-free bifunctional carbon electrocatalysts derived from zeoliticimidazolate frameworks for efficient water splitting. *Mater. Chem. Front.* **2018**, *2*, 102−111.
(55) Li, X.; Niu, Z.; Jiang, J.; Ai, L. Cobalt nanoparticles embedded in porous N-rich carbon as an efficient bifunctional electrocatalyst for water splitting. *J. Mater. Chem. A* **2016**, *4*, 3204−3209.
(56) Park, S. W.; Kim, I.; Oh, S. I.; Kim, J. C.; Kim, D. W. Carbon-encapsulated NiFe nanoparticles as a bifunctional electrocatalyst for high-efficiency overall water splitting. *J. Catal.* **2018**, *366*, 266−274.
(57) Wang, J.; Gao, D.; Wang, G.; Miao, S.; Wu, H.; Li, J.; Bao, X. Cobalt nanoparticles encapsulated in nitrogen-doped carbon as a bifunctional catalyst for water electrolysis. *J. Mater. Chem. A* **2014**, *2*, 20067−20074.
(58) Wen, X.; Yang, X.; Li, M.; Bai, L.; Guan, J. Co/CoO_x nanoparticles inlaid onto nitrogen-doped carbon-graphene as a trifunctional electrocatalyst. *Electrochim. Acta* **2019**, *296*, 830−841.
(59) Wu, Z. Y.; Ji, W. B.; Hu, B. C.; Liang, H. W.; Xu, X. X.; Yu, Z. L.; Li, B. Y.; Yu, S. H. Partially oxidized Ni nanoparticles supported on Ni-N co-doped carbon nanofibers as bifunctional electrocatalysts for overall water splitting. *Nano Energy* **2018**, *51*, 286−293.
(60) Xi, W.; Ren, Z.; Kong, L.; Wu, J.; Du, S.; Zhu, J.; Xue, Y.; Meng, H.; Fu, H. Dual-valence nickel nanosheets covered with thin carbon as bifunctional electrocatalysts for full water splitting. *J. Mater. Chem. A* **2016**, *4*, 7297−7304.
(61) Fan, H.; Yu, H.; Zhang, Y.; Zheng, Y.; Luo, Y.; Dai, Z.; Li, B.; Zong, Y.; Yan, Q. Fe-doped Ni_3C nanodots in N-doped carbon nanosheets for efficient hydrogen-evolution and oxygen-evolution electrocatalysis. *Angew. Chem., Int. Ed.* **2017**, *56*, 12566−12570.
(62) Yang, Z.; Zhao, C.; Qu, Y.; Zhou, H.; Zhou, F.; Wang, J.; Wu, Y.; Li, Y. Trifunctional Self-Supporting Cobalt-Embedded Carbon Nanotube Films for ORR, OER, and HER Triggered by Solid Diffusion from Bulk Metal. *Adv. Mater.* **2019**, *31*, No. 1808043.
(63) Yang, C. C.; Zai, S. F.; Zhou, Y. T.; Du, L.; Jiang, Q. Fe_3C-Co nanoparticles encapsulated in a hierarchical structure of N-Doped carbon as a multifunctional electrocatalyst for ORR, OER, and HER. *Adv. Funct. Mater.* **2019**, *29*, No. 1901949.
(64) Yin, T.; Zhou, X.; Wu, A.; Yan, H.; Feng, Q.; Tian, C. CoP particles embedded in N-doped two-dimensional carbon sheets as efficient electrocatalyst for water splitting. *Electrochim. Acta* **2018**, *276*, 362−369.
(65) Zhou, Z.; Mahmood, N.; Zhang, Y.; Pan, L.; Wang, L.; Zhang, X.; Zou, J. J. CoP nanoparticles embedded in P and N co-doped carbon as efficient bifunctional electrocatalyst for water splitting. *J. Energy Chem.* **2017**, *26*, 1223−1230.

https://doi.org/10.1021/acsomega.1c00641
ACS Omega 2021, 6, 12623−12630